Engineered Science
DOI: https://dx.doi.org/10.30919/es1286

Computational Studies on Carbazole-Pyranocoumarin Conjugate Against α-glucosidase Enzyme

Muhammad Ikhlas Abdjan,[1] Nanik Siti Aminah,[1, 2,*] Alfinda Novi Kristanti,[1, 2] Imam Siswanto,[1, 3] Axl Laurens Lukas Windah,[1] Tin Myo Thant,[4] Rico Ramadhan,[1] Yoshiaki Takaya,[5] Zaheer Ul-Haq,[6] Muhammad Iqbal Choudhary[7]

Abstract

α-Glucosidase is an enzyme responsible for releasing the α-D-glucose monomer through hydrolysis reactions. The release of this monomer increases the sugar concentration in the blood and increases the risk of type-2 diabetes mellitus (DM) patients. Through computational studies, we evaluate the structural and inhibitory efficiency of the new carbazole-pyranocoumarin conjugate/Carbazomarin-C as α-Glucosidase inhibitor at the molecular level. We found that Carbazomarin-C (Car) has promising drug-likeness and ADMET properties. Meanwhile, proton chemical shift modeling through a density functional theory (DFT) approach shows that the Car molecule had an agreement with experimental results. Molecular dynamics simulation was applied to understand their inhibitory efficiency through free energy binding (ΔGbind and ΔGexp). The results showed that Car (ΔGbind: -6.10 kcal/mol and ΔGexp: -5.02 kcal/mol) had better inhibition than Acarbose as a control (ΔGbind: -4.48 kcal/mol and ΔGexp: -3.17 kcal/mol). Moreover, nine residues were responsible for the bond stabilization of both inhibitors, namely F175, R210, V213, Q276, F300, P309, L310, R439, and R443. The information in this work demonstrated how potential Carbazomarin-C is as an α-Glucosidase inhibitor at the molecular level.

Keywords: α-glucosidase; Carbazole-pyranocoumarin; Molecular modeling; Molecular docking; Molecular dynamics simulation.
Received: 20 February 2024; Revised: 17 June 2024; Accepted: 06 July 2024.
Article type: Research article.

1. Introduction

Diabetes is a disease characterized by chronic hyperglycemia and insulin disorders, which result in metabolic changes that affect all body tissues.[1,2] Meanwhile, hyperglycemia is a condition that decreases the insulin sensitivity of pancreatic β cells.[3] The impact of decreasing insulin causes blood sugar levels to be unconverted to muscle and fat tissues.[4] It can happen because the pancreas organ cannot produce insulin like usual. As a result, the sugar concentration in the blood has increased in type-2 diabetes mellitus (DM-2) patients. This condition causes the body's metabolism of DM-2 patients to be unable to control the glucose molecules from the carbohydrates consumed. The effects caused by diabetes are heart attacks,[5,6] artery narrowing,[5,6] and strokes.[7]

Previous research shows that there are several enzymes responsible for diabetes, including angiotensin-converting enzyme (ACE),[8] dipeptidyl peptidase IV (DPP-IV),[9] α-glucosidase,[10] and α-amylase.[11] ACE and DPP-IV enzymes are considered crucial in regulating blood pressure and blood sugar. In addition, both enzymes regulate the control of hypertension and diabetes at the same time.[12] Meanwhile, α-glucosidase and α-amylase are known digestive enzymes that function to break down carbohydrates (poly/oligo/di-saccharides) into their monomers.[13] The involvement of those enzymes becomes a targeted protein that leads to reduced diabetes by controlling blood sugar concentration. In particular, α-glucosidase is the main target in this research because of its ability to increase blood sugar concentration through carbohydrate hydrolysis reactions.[14]

The hydrolysis of carbohydrates (oligosaccharides and disaccharides) into glucose molecules is mediated by the α-glucosidase enzyme. This enzyme from the carbohydrase class plays a role in catalyzing the release of α-D-glucose molecules

[1] *Department of Chemistry, Faculty of Science and Technology, Universitas Airlangga, Komplek Kampus C UNAIR, Jl. Mulyorejo, Surabaya 60230, Indonesia.*
[2] *Biotechnology of Tropical Medicinal Plants Research Group, Universitas Airlangga, Surabaya 60230, Indonesia.*
[3] *Bioinformatic Laboratory, UCoE Research Center for Bio-Molecule Engineering, Universitas Airlangga, Surabaya 60230, Indonesia.*
[4] *Department of Chemistry, Kyaukse University, Kyaukse Township 10014, Myanmar.*
[5] *Faculty of Pharmacy, Meijo University, 150 Yagotoyama, Tempaku, Nagoya 468-8503, Japan.*

into the bloodstream.[14] The location of the α-glucosidase enzyme is in the small intestine area. Specifically, it is located on the surface of epithelial cells (Fig. 1). This enzyme is bound to the surface of the bilayer membrane of epithelial cells and aims to break down carbohydrates into α-D-glucose monomers to be continued in the bloodstream.[15,16] The process of breaking down carbohydrates is carried out by this enzyme through a hydrolysis reaction by breaking the α-(1,4)-glycosidic linkage of carbohydrates to become its monomer (α-D-glucose.) Food and nutrients in the form of carbohydrates (disaccharides and oligosaccharides) that enter through the small intestine will be absorbed by epithelial cells. However, these carbohydrates need to be broken down into their monomers, α-D-glucose, which aims to enter through the integral protein sodium-couple glucose transporters (SGLT). The transporting process of the α-D-glucose molecule requires the help of two sodium ions (Na^+) to enter the epithelial cells through the SGLT protein.[16,17] Therefore, salt levels in the body of DM-2 patients need to be reduced. It aims to control the process of absorption of glucose molecules into the epithelial cells by sodium ions. Then, the α-D-glucose can be passed through the integral glucose transporters-2 (GLTU2) protein to enter the blood vessels (Fig. 2).

Excessive activity of this enzyme causes the release of α-D-glucose molecules, which are absorbed by the intestinal lumen and enter through the blood circulation. Therefore, inhibition of the α-glucosidase enzyme is expected to stop the regulatory process of hydrolyzing carbohydrates into their monomers.[18,19] The α-glucosidase enzyme inhibitors act as competitive inhibitors.[18] Acarbose is a commercially available inhibitor of the α-glucosidase enzyme and is known to have good inhibitory activity.[20,21] However, several previous studies reported that acarbose can cause diarrhea and irritation of the small intestine wall. Therefore, the development of α-glucosidase enzyme inhibitors needs to be studied to find safer and more effective drug candidates.

Natural products offer an opportunity to discover a new drug candidate that is safe and effective because of their chemical structure diversity. One of them is the new carbazol-pyranocumarin conjugate (Carbazomarin-C), which was successfully isolated and characterized from *Calusena excavata* roots.[22] Carbazomarin-C is a secondary metabolite compound consisting of two main structures, namely carbazole alkaloid and coumarin (Fig. 3). The two main structures are connected by the C6-C6" bond. Moreover, several functional groups are present in the structure of this compound, such as hydroxyl (-OH), ketones (C=O), aldehydes (CHO), and amines (NH). Those functional groups are expected to increase their biological activity.[23] Coumarin structure has been identified as having activity as a-glucosidase inhibitor. Our previous work has identified several coumarins having promising activity as α-glucosidase inhibitors.[24,25] Besides, another report shows that carbazole alkaloids provide good potency as α-glucosidase inhibitors.[26] These two main structures are one of our considerations in looking at the potential of Carbazomarin-C as a potential α-glucosidase inhibitor. We suspect that combining both main structures into the structure-activity relationship (SAR) can provide even better inhibitory activity against α-glucosidase. Previous research reported that Carbazomarin-C (IC_{50}: 0.22 mM) had promising activity in inhibiting α-glucosidase enzyme activity compared to acarbose (IC_{50}: 4.89 mM) as a positive control.[22] Based on these results, Carbazomarin-C and acarbose compounds were chosen as the main focus of this work to understand their inhibitory activity at the molecular level. The chemical structure of acarbose is shown in Fig.S1.

Computational studies have advantages in studying the activity of a compound efficiently, systematically, and comprehensively.[27–30] Some information on compound activity can be evaluated, such as physicochemical properties, quantum chemical properties, and inhibitory mechanisms at the molecular level. Based on previous studies, *in vitro* approach to the activity of the Carbazomarin-C against α-glucosidase has been reported.[22] However, their activity and inhibitory mechanisms at the molecular level have not been reported. Therefore, this work aims to theoretically investigate the activity of Carbazomarin-C as an α-glucosidase inhibitor through computational studies (*in silico*). Several *in silico* approaches were applied, such as physicochemical prediction, density functional theory (DFT), molecular docking, and molecular dynamics (MD) simulation. Those approaches aim to study several variables dealing with the interaction between inhibitors and α-glucosidase in the form of initial coordinates, dynamics behavior, pocket area interaction, and inhibitory efficiency. In addition, several drug-likeness, ADMET (absorption, distribution, metabolism, excretion, and toxicity), and electronic structure criteria are needed for further evaluation of the activity purpose of Carbazomarin-C. We hope the obtained information in this work can be useful for future drug discovery of more specific inhibitors from natural products for DM-2 patients' treatment.

2. Experimental section

2.1 Pharmacokinetic predictions

Carbazomarin-C (Car) is a compound that is the main focus of this study to predict its pharmacokinetic properties in the form of bioavailability and ADMET properties. The predicting small-molecule pharmacokinetic properties using graph-based signatures or pkCSM server is used to view the ADMET properties of the modeled compound.[31] Meanwhile, the bioavailability properties are calculated using the SwissADME web service server.[32] All calculations use the

[6] *Dr. Panjwani Center for Molecular Medicine and Drug Research, International Center for Chemical and Biological Sciences, University of Karachi, Karachi 75270, Pakistan.*

[7] *H. E. J. Research Institute of Chemistry, International Center for Chemical and Biological Sciences, University of Karachi, Karachi 75270, Pakistan.*

**Email:* nanik-s-a@fst.unair.ac.id (N. S. Aminah)

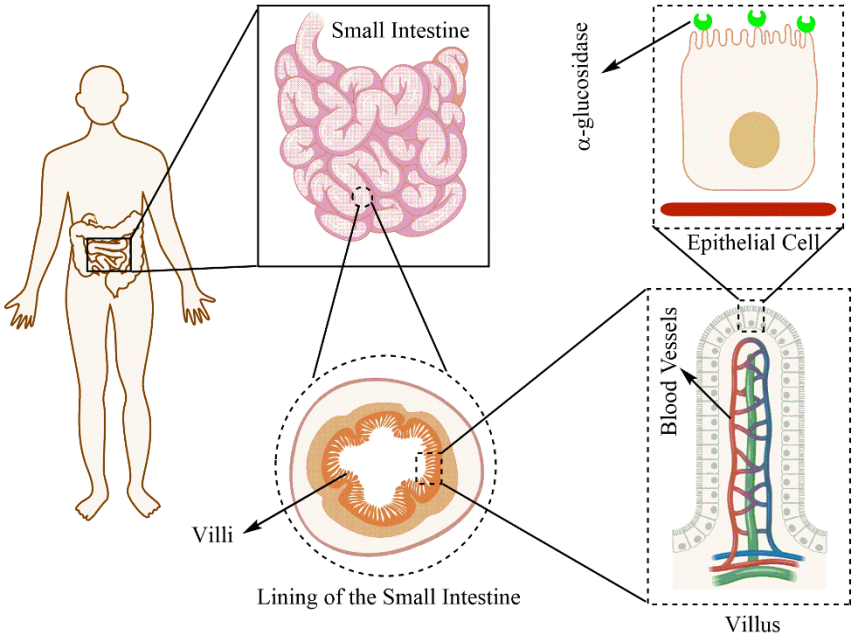

Fig. 1 Location of the α-glucosidase enzyme on the epithelial cells surface.

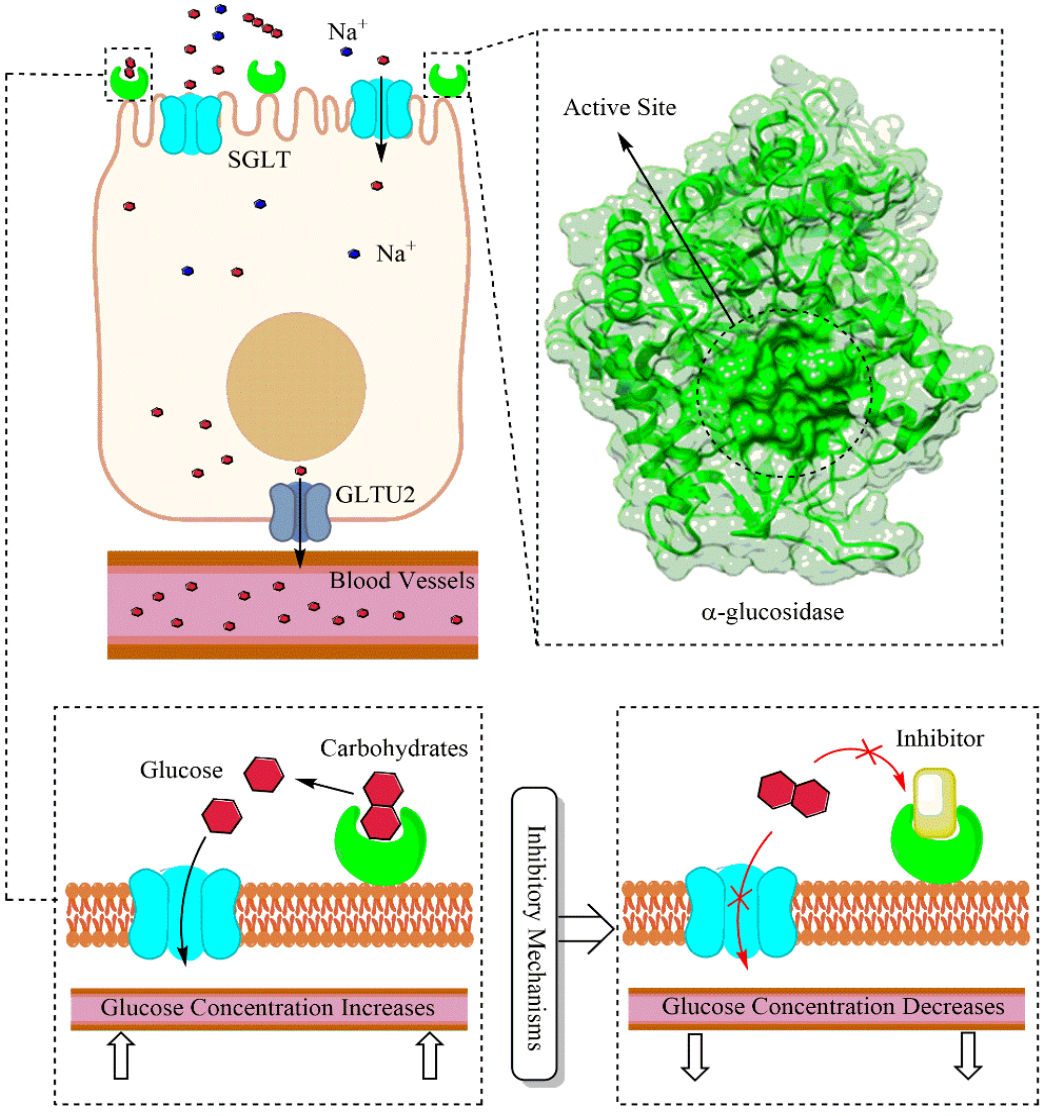

Fig. 2 The mechanism of releasing glucose molecules into the blood vessels and the inhibitory mechanism of the α-glucosidase enzyme by inhibitors.

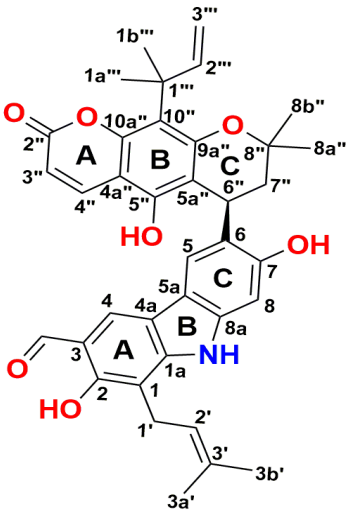

Fig. 3 The chemical structure of Carbazomarin-C (Car) and its label.

input file in SMILES format.

2.2 Quantum chemical modeling

Quantum chemical properties were calculated by using the Gaussian 16W package.[33] Geometry optimization was performed using the DFT method with a Becke 3-parameter hybrid functional Lee-Yang-Par (B3LYP).[34] Moreover, the 6-311++G(d,p) basis set was applied to calculate the electrostatic potential (ESP) charge. The optimized structure (Fig. S2) is used for further analysis in the form of proton chemical shift (^{1}H-NMR) calculations. The gauge independent atomic orbital (GIAO) approach[35] was applied to calculate the 1H-NMR in the gas and solvation phases. The solvent model used is chloroform with integral equation formalism of polarizable continuum model (IEFPCM). TMS shielding at the GIAO/B3LYP/6-311+G(2d,p) level of theory as a reference to calculate the ^{1}H-NMR of modeled structure. For evaluation purposes, we used statistical analysis in the form of correlation and accuracy of ^{1}H-NMR between experimental and theoretical.[36,37] Some of the parameters analyzed are determination coefficient (R^2 and R_0^2), absolute error/MAE (Eqn. 1), root mean square error/RMSE (Eqn. 2), and mean absolute percentage error/MAPE (Eqn. 3).

$$MAE = \frac{1}{n} \sum_{i=1}^{n} |\delta_i^{theo} - \delta_i^{exp}| \quad (1)$$

$$RMSE = \sqrt{\frac{1}{n} \sum_{i=1}^{n} (\delta_i^{theo} - \delta_i^{exp})^2} \quad (2)$$

$$MAPE = \frac{\sum_{i=1}^{n} \left| \frac{\delta_i^{theo} - \delta_i^{exp}}{\delta_i^{exp}} \right|}{n} \times 100 \quad (3)$$

2.3 System preparation: Data sets, molecular docking, topology, and minimization

α-glucosidase as a targeted protein is an enzyme that is responsible for regulating the release of α-glucose molecules in DM-2 patients following the previously described in the introduction section. α-glucosidase enzyme from *Saccharomyces cerevisiae* was selected as the targeted protein from the protein data bank (PDB ID: 3A4A) (https://www.rcsb.org/structure/3a4a). On the pocket site of the co-crystal, there is a native ligand, namely α-D-glucopyranose (PDB ID: GLC).[38] That ligand is used to determine the α-glucosidase active site. Missing residue on the receptor was rebuilt using Modeller 9.21 package. The optimized structure of Carbazomarin-C (Car) is used for molecular evaluation purposes by looking at its interaction with α-glucosidase. In this research, we also used acarbose (Aca) as a positive control. Furthermore, receptor (α-Glu) and inhibitors (Aca and Car) were calculated for several parameters, such as bonded, non-bonded, and charge through the Chimera 1.13 package.

The α-glucosidase active site was determined through a redocking step using the DOCK6 package. As described in our previous research, several crucial parameters used in the redocking step are grid spacing, center, and dimension.[39] In detail, the redocking parameters used are grid spacing (0.3 Å), center (X: 20.53, Y: -10.11, and Z: 22.38), and dimension (X: 27.31, Y: 29.51, and Z: 29.35). To validate the parameters, the root-mean-square deviation (RMSD) should fulfill the criteria with RMSD ≤ 2.00 Å. The obtained superposition from the RMSD value met the criteria, which is 0.99 Å. Furthermore, the obtained coordinates from the redocking step are used for the docking inhibitors process. The docking inhibitors step aims to get the initial coordinates before the evaluation step is carried out using the MD simulation. The interaction energy in the gas phase uses the grid score function approach.[40,41] In detail, the grid score (Eqn. 4) is obtained from van der Waals (E_{vdW}) and electrostatic (E_{ele}) energies.

$$Grid\text{-}score = E_{vdW} + E_{ele} \quad (4)$$

The obtained coordinates from molecular docking are used to create a topology system. Here, we use the *tleap* tool in the AMBER22 package to build each topology as a ligand, receptor, complex, and solvated complex.[42] Several additional parameters are crucial in making the system topology, such as the AMBER force field (FFSB14), water solvent model (TIP3PBOX with a distance of 12 Å), and counter ions (Na^+) were applied. This stage aims to obtain coordinates and parameters used for simulation purposes in the form of *prmtop* and *inpcrd* files.

To reduce bad contact and stress hindrances in the system. A minimization step is needed to eliminate these weaknesses.[43] The system minimization process goes through three minimization steps, following water molecules and sodium ions, ligand-receptor, and the whole system. In addition, the steepest descent (maxcyc) of 1500 steps and the conjugate gradient (ncyc) of 500 steps were applied. The entire calculation process uses the *sander* tool available in the AMBER22 package.[44] The system minimization results obtained from this stage are used for further calculation processes in the MD simulation

2.4 Molecular dynamics simulation

The simulation process is carried out through several steps in the form of heating, equilibrium, and production. The heating step was simulated for 200 ps with a gradual temperature from 10 K to 300 K. Next, the system was equilibrated for 1300 ps with harmonic restraints of 30, 20, 10, and 5 kcal/mol/Å^2. Finally, the whole system was produced under NPT ensemble conditions with pressure (1 atm) and temperature (310 K) constant for 200 ns. Trajectories were saved every 1000 ps per trajectory at the production step. The entire calculation process uses the *PMEMD.cuda* tool available in the AMBER22 package.[45] The simulation steps aim to create trajectories that are used for further analysis purposes

2.5 Trajectories analysis

Trajectories were analyzed using several tools available in the AMBER22 package in the form of *process_mdout.perl*,[46] *cpptraj*,[47] and *MMPBSA.py*.[48] Several variables evaluated are dynamics behavior, pocket area interaction, and inhibitory efficiency. Specifically, dynamics behavior and pocket area interaction were analyzed using 200 ns trajectories. Meanwhile, inhibitory efficiency and key binding residue in the form of free energy binding (ΔG_{bind}) and energy decomposition ($\Delta G_{bind}^{residue}$) were analyzed using the last 20 ns (180-200 ns) of trajectories. This consideration is taken based on efficiency cost and time calculation. Moreover, this consideration is used if each system has achieved good stability, which will be explained in the results and discussion section.

Mechanics/Molecular-Poisson Boltzmann Surface Area (MM-PBSA) approach was used to calculate enthalpy (ΔH),[48,49] which is the contribution of free energy in the gas (ΔG_{gas}) and solvation (ΔG_{solv}) phases (Eqn. 5). In detail, the contribution of ΔG_{gas} and ΔG_{solv} show by Eqns. 6 and 7. In particular, bonded energy (ΔE_{bonded}) shows bond, angle, and torsion, which have conformational energy equal to zero. Thus, several energy components that influence the ΔH value consist of van der Waals (ΔE_{vdW}), electrostatic (ΔE_{ele}), Poisson Boltzmann model (ΔG_{solv}^{ele}), and solvent-accessible surface area energy ($\Delta G_{solv}^{nonpolar}$). The entropy change ($-T\Delta S$) was calculated by the normal mode approximation (NMODE).[48,50] Finally, we can calculate the ΔG_{bind} using some parameters that describe in Eqns. 8 and 9. Meanwhile, we also calculate the free energy binding experiment (ΔG_{exp}) using the IC_{50} value as a reference.[51] In detail, all variables are described by Eqn. 10. The variables R and T are the ideal gas constant (1.9872 X 10^{-3} kcal/mol.K) and room temperature (300 K), respectively. The ΔG_{bind} and ΔG_{exp} were calculated to see their inhibitory efficiency against α-glucosidase, thermodynamically.

$$\Delta H = \Delta G_{gas} + \Delta G_{solv} \quad (5)$$

$$\Delta G_{gas} = \Delta E_{bonded} + \Delta E_{vdW} + \Delta E_{ele} \quad (6)$$

$$\Delta G_{solv} = \Delta G_{solv}^{ele} + \Delta G_{solv}^{nonpolar} \quad (7)$$

$$\Delta G_{bind} = \Delta H - T\Delta S \quad (8)$$

$$\Delta G_{bind} = \Delta E_{vdW} + \Delta E_{ele} + \Delta G_{solv}^{ele} + \Delta G_{solv}^{nonpolar} - T\Delta S \quad (9)$$

$$\Delta G_{exp} = R.T.\ln(IC_{50}) \quad (10)$$

3. Results and discussion

3.1 Carbazomarin-C: Drug-likness and ADMET

Drug-likeness and ADMET prediction of the Car compound provided initial information on the criteria for a viable drug. The drug-likeness criteria have been described by the Lipinski[52] and Veber[53] rules. In detail, the prediction of drug-likeness is shown in Table 1. Overall, the Car has only one violation, namely in the parameter MW ≥ 500 g/mol. It can be understood due to the combined structure of carbazoles and alkaloids, which are conjugated through the C6-C6" bond. Consequently, it can increase its molecular weight (MW). Meanwhile, other parameters such as M LogP, ∑HBD, ∑HBA, rotatable bonds, and TPSA still meet the criteria for a good drug candidate. These findings identify that Car still has a molecular structure with a reliable drug-likeness category as a promising drug candidate. It is also supported by its bioavailability score, which is 0.55. It should be noted that the bioavailability criterion is declared good if it has a score of 0.55-0.56.[54] Briefly, this parameter is a crucial consideration to determine the criteria for a good drug.

ADMET prediction is advantageous in providing drug information when consumed in the body. This information is useful for assessing the pharmacokinetic properties of drugs. Several crucial ADMET parameters are Caco-2 permeability, human small intestine (HIA), blood-brain barrier (BBB), total clearance, renal OCT2 substrate, cytochrome isoenzymes (CYP), AMES toxicity, and hepatotoxicity.[31] In detail, we provide predictive information from ADMET properties using the pkCSM server web service (Table 2). Overall, the predictions of ADMET for Car show promising potential as a drug candidate. In particular, for metabolism and toxicity parameters, Car does not interfere with cytochrome isoenzymes. Also, it is defined as a non-toxic category. The information presented in this section is initial predictions to see the pharmacokinetic properties of the Car compound. However, the information presented can provide insight and initial consideration before conducting clinical trials on the ability of this compound.

3.2 Proton chemical shift of Carbazomarin-C

Proton Chemical shift (^{1}H-NMR) was modeled using the DFT/GIAO/B3LYP/6-311+G(2d,p) method on gas and solution (chloroform-IEFPCM) phases. The ^{1}H-NMR modeling is considered more sensitive in determining the dominant fingerprint criteria of the molecular structure in solution.[37,55] To identify the displacement of each proton in

the molecular structure of Car, we have labeled its structure (Table 1 and Fig. S2).

Table 1. Drug likeness and bioavailability prediction of Car using Swiss ADME server.

Parameters	Car
Lipinski	
MW (g/mol)	607.69
M LogP	3.75
∑HBD	4
∑HBA	7
Veber	
Rotatable bonds	6
TPSA (Å^2)	132.99
Violations/n	1
Bioavailability Score	0.55

Lipinski rule: MW ≤ 500 (g/mol), MlogP ≤ 4.15, ∑ HBA ≤ 10 dan ∑ HBD ≤ 5 and Veber rule: ∑ Rotatable bonds ≤ 10 dan TPSA ≤ 140 Å^2

Table 2. ADMET prediction of car using pkCSM server.

Parameters	Car
Absorption	
Caco-2 Permeability (log Papp in 10^{-6} cm/s)	0.70
Intestinal Absorption-Human (% Absorbed)	100
Distribution	
BBB Permeability (log BB)	-1.51
Metabolism	
CYP1A2 Inhibitor	No
CYP2D6 Inhibitor	No
Excretion	
Total Clearance (log mL/min/Kg)	-1.20
Renal OCT2 Substrate	No
Toxicity	
AMES toxicity	No
Hepatotoxicity	No

Hight Caco-2 permeability > 0.90, Intestinal Absorption-Human (+HIA > 30% and -HIA < 30%), and BBB Permeability (+log BB > 0.30 and -log BB < -1.00).

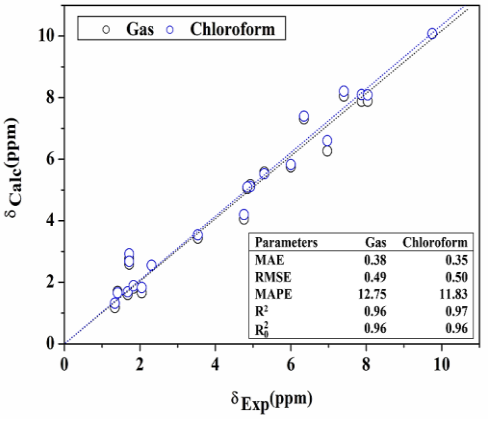

Fig. 4 The Car proton chemical shift between experimental (δ_{Exp}) and theoretical (δ_{Calc}). The ^{1}H-NMR was calculated using the B3LYP/6-311++G(2d,p) level of theory as a reference. Statistical analysis was performed to see their correlation and accuracy.

The ^{1}H-NMR Car was obtained from our previous studies.[22] In detail, the ^{1}H-NMR data are shown in Table S1. The modeling results show that the experimental and theoretical ^{1}H-NMR have good correlation and accuracy (Fig. 4). It is supported by several statistical parameters. Linear regression analysis shows the value of R^2 and $R_0^2 \geq 0.90$, with linear equations y= 0.9853x + 0.1921 (gas) and y= 0.9933x + 0.254 (solution). These results identify that the experimental and theoretical ^{1}H-NMR data do not have significant shift values in the gas and solution phases. Furthermore, we also perform statistical analysis for accuracy parameters in the form of MAE, RMSE, and MAPE. The smaller the parameter value, the better the accuracy results.[37] In particular, MAPE parameters are one of the most reliable model equations in representing the accuracy of a model. The MAPE parameter results show the ^{1}H-NMR modeling in gas and solution phases ≤ 20%. It identifies that the modeling results are in the range of the good forecasting category. The output data obtained from this section aims to obtain a reliable optimized structure for further analysis using a structure-based approach.

3.3 Initial coordinate determination

The molecular docking step aims to obtain the initial coordinates based on the coordinates of the native ligand. Determination of the active site using molecular docking makes it efficient to get the orientation of each inhibitor.[56] Here, we use the redocking parameter to determine the α-glucosidase active site based on the parameters from previous studies.[39] The obtained parameters were used for docking inhibitors (Aca and Car).

The orientation and grid score of each inhibitor are shown in Fig. 5. The results show that the grid score is influenced by the contribution of energy in the gas phase, in the form of E_{vdW} and E_{ele}. In detail, each energy contribution (kcal/mol), namely Aca-α-Glu (E_{vdW}: -30.39 and E_{ele}: -21.39) and Car-α-Glu (E_{vdW}: -36.52 and E_{ele}: -22.38). Additionally, several amino acid residues are responsible for the inhibitor-α-glucosidase interaction (Fig. S3). It can be seen that the amino acid residues responsible for the interaction of the inhibitors are Aca-α-Glu (seven residues: K153, D304, P309, L310, R312, D349, and R439) and Car-α-Glu (nine residues: K153, Y155, G157, E274, H277, F300, D304, R312, and Y344). These interactions are in the form of conventional hydrogen bonds, carbon-hydrogen bonds, alkyl, and pi-alkyl interactions (Table S2). Interestingly, the Car orientation at the receptor active site, the carbazole region provides significant interactions with several amino acids compared to the coumarin region. Mainly, the interaction of hydrogen bonds following by Car-α-Glu (carbazol: 7C-OH…D304(OD1) and 2C-OH…E274(OE2) and coumarin: G157(HN)…2"C=O). Additionally, the hydrogen bond type in the carbazol region is hydrogen bond donor (HBD). Besides, the coumarin region is a hydrogen

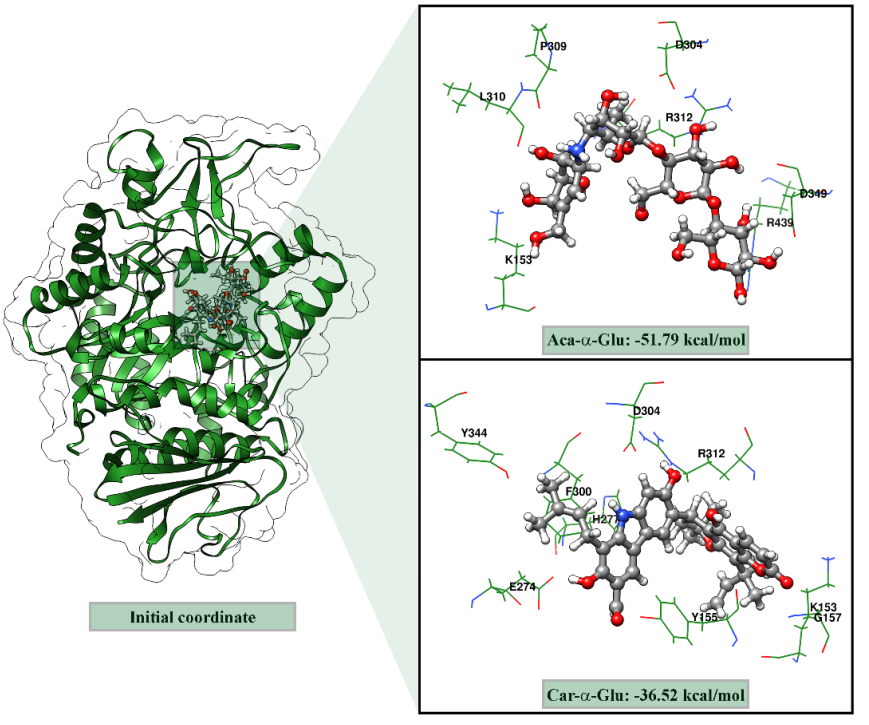

Fig. 5 The orientation and grid score analyses by molecular docking: Each inhibitor binding well on the α-glucosidase active site.

bond acceptor (HBA). Several details of the differences in interactions in each region of the Car molecule are influenced by the presence of functional groups in the form of hydroxy (-OH) and ketone (C=O). We suspect that the presence of the –OH functional group contributes the most to the H-bond interaction in the form of HBD. It can be seen from the positive control interaction (Aca-α-Glu), which is more dominant in terms of the hydrogen bond interaction compared to the Car-α-Glu interaction. However, molecular docking analysis is an initial step in obtaining the initial orientation.[57] Thus, an MD simulation analysis is needed to provide insight that advances in studying the interaction between inhibitors and α-glucosidase at the molecular level. It will be discussed in the next section.

3.4 Dynamics behavior: Quality, stability, rigidity, and flexibility

The obtained orientation from molecular docking was integrated into the MD simulation using the general amber force field (GAFF).[58] Here, we create three dissolved systems to perform the simulation process, followed by Apo protein (α-Glu) and complex-solvated (Aca-α-Glu and Car-α-Glu). Trajectories generated during the 200 ns simulation process are used to evaluate the dynamics behavior for all systems, such as quality, stability, rigidity, and flexibility.

Convergence analysis is performed to see the system quality during the simulation process. Some of the variables analyzed are density (g/mL), pressure (bar), temperature (K), and total energy (kcal/mol). All analysis of these variables uses the *process_mdout.perl* tool available in the AMBER22 package. The results show that all systems have converged and reached equilibrium. It can be identified in Fig. S4, which does not show significant fluctuations in each variable measured. In addition, this opinion is supported by differences in the average values that are not significant in each system (Table

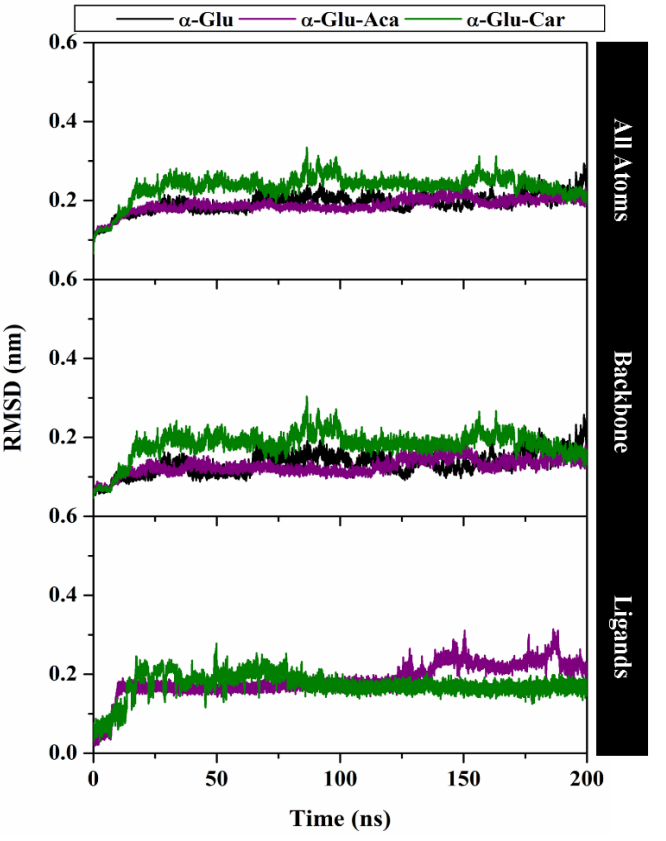

Fig. 6 The root-mean-square displacement of all atoms, backbone, and ligand plotted along 200 ns of MD simulation.

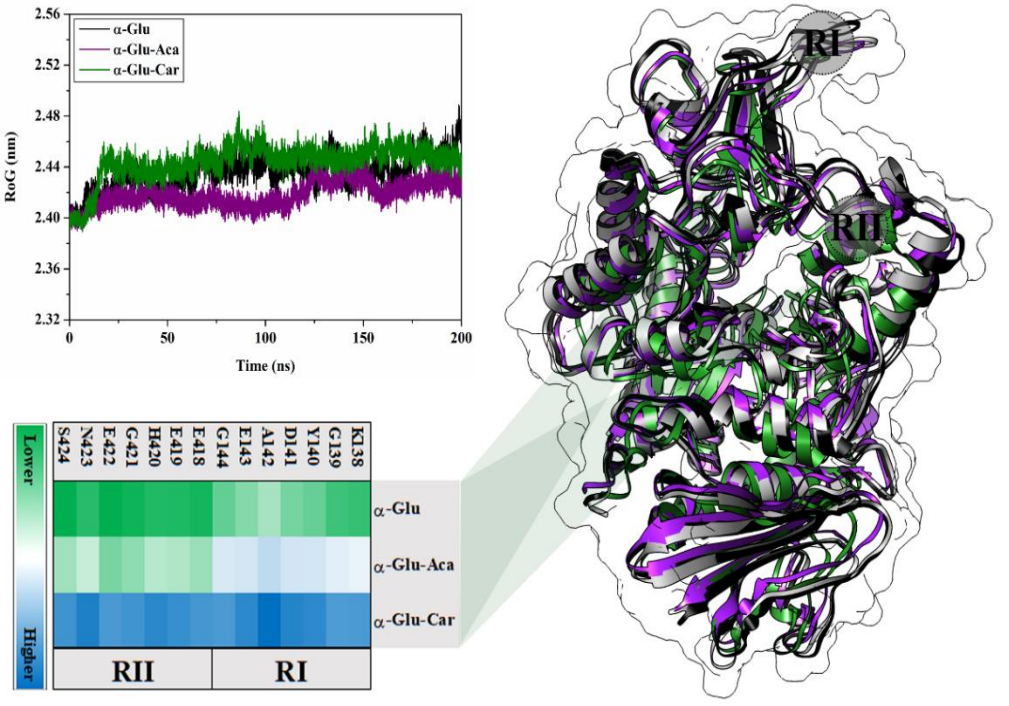

Fig. 7 Trajectories analysis along 200 ns of MD simulation are shown by radius of gyration (RoG), root-mean-square fluctuation (RMSF), and average structure.

S3). These findings identify that the simulation process carried out for 200 ns on each system is feasible for further analysis.

The root-mean-square of displacement (RMSD) value identified the system stability during the simulation time.[59] Separately, we performed RMSD analysis in the form of all atoms, backbone (BB), and ligands. It aims to see how the level of stability in each variable becomes a concern in this stage. Overall, the fluctuation values of each RMSD (all atoms, BB, and ligand) in all systems showed RMSD fluctuations ≤ 0.4 nm. It can be seen in Fig. 6 and Table S3. The RMSD fluctuation value indicates that the system has achieved good stability. Moreover, the RMSD fluctuations of all atoms in the Apo and complex systems did not show significant differences in fluctuations (~0.18 to ~0.23 nm). It identified that the structure of α-glucosidase without and with the inhibitor did not experience a significant change in coordinates. Fluctuation changes (all atoms RMSD) start at 0-15 ns and start to equilibrate until the end of the simulation. These fluctuations can occur due to adjusting the system to achieve stability, which is influenced by several parameters, such as temperature, pressure, density, and energy minimization at the beginning of the simulation. In particular, the last 20 ns trajectories (180-200 ns) show good stability for each system. Those trajectories will be used to analyze the free energy binding (ΔG_{bind}) and energy decomposition ($\Delta G^{residue}_{bind}$), which will be discussed in the next section.

The dynamics behavior evaluation stage is continued by looking at the flexibility of each system as indicated by the B-factor and root-mean-square fluctuation (RMSF).[60] It can be seen that the Apo-proteins are less flexible than their complexes (Fig. S5). It is supported by the average value of B-factor and RMSF for each system in order of flexibility, followed by α-Glu < Aca-α-Glu < Car-α-Glu (Table S3). Specifically, higher flexibility occurs in the loop (RI: 138-144) and helix (RII: 418-424) regions (Fig. 7). Overall, changes in fluctuations in the value of flexibility do not affect the α-glucosidase active site in each system. It is important to note that pocket changes during simulation can affect the orientation and binding affinity of the receptor-ligand. We also carried out a radius of gyration (RoG) analysis to see the system's compactness.[61] The results show that each system has good rigidity because it has an RoG value that is not too significant (Fig. 7 and Table S3). To see the correlation between the flexibility and rigidity of each system, we extracted the average structure of 200 ns trajectories that were colored by Grey: co-crystal, black: α-Glu, purple: Aca-α-Glu, and forest green: Car-α-Glu (Fig. 7). The superposition of each system suggests that the structure of the standard residue is well-folded. It can be seen that there is no significant change between the co-crystal structure (PDB) and all systems. Based on the described above, the dynamic behavior of each system has reached equilibrium and is suitable for further analysis.

3.5 Pocket area interaction: Water accessibility, atomic contact, and hydrogen bond

For the following analysis, we tried to look at pocket area interactions, such as water accessibility, atomic contact, and hydrogen bond (H-bond) (Fig. 8). The analysis variables were extracted from 200 ns trajectories using the *cpptraj* tool in the AMBER22 package. In this section, we focus on looking at ligand-receptor interactions. The data obtained from this analysis is expected to provide information regarding the

ability of the inhibitor to access the pocket area on the α-glucosidase surface.

The solvent-accessible surface area (SASA) was used to see the ability of water molecules to access the receptor pocket area.[62] Commonly, water molecules play a role in maintaining protein structure.[63] The results show the SASA value of Car-α-Glu higher access by water molecules comparing Aca-α-Glu. In detail, the average value of SASA is Aca-α-Glu: 4.23 ± 2.22 nm^2 and Aca-α-Glu: 11.42 ± 2.78 nm^2. The difference in the orientation of the inhibitor in the binding pattern in the pocket area affects the number of water molecules accessing it. We suspect that each inhibitor's orientation changes during the simulation process (heating to equilibrium). The heating is performed gradually, from 10 K to 300 K. Molecules move randomly at a rate determined by their mass, environment (in this case, water molecules), and the amount of thermal energy they possess, which is proportional to temperature. This movement explains the molecule's dynamic behavior through the medium in which they are situated. Next, the system is equilibrated periodically through decreasing harmonic restraint. This step causes the inhibitor molecule to seek a stable binding orientation at the α-Glu pocket site. Consequently, the free space in the pocket area is occupied by water molecules. It should be noted that the SASA analysis uses a radius of 5 Å from the coordinates of each inhibitor.

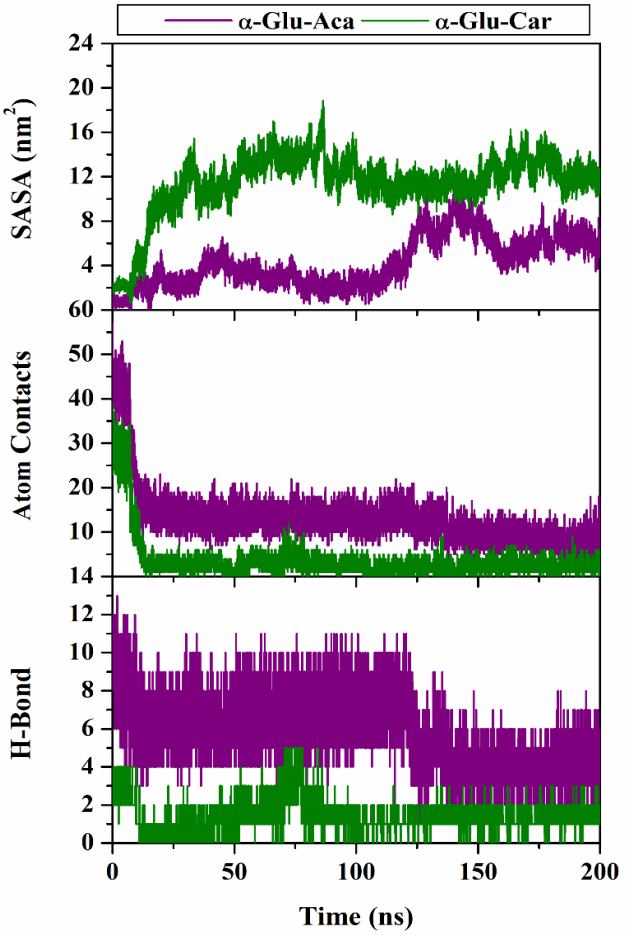

Fig. 8 Pocket area interactions were plotted along 200 ns trajectories using the *cpptraj* tool.

Table 3. Hydrogen bonds analysis using 20800 frames from the last 20 ns trajectories. The cut value: distance 3.5 Å and angle 120°.

H-Bond Interaction	PO (%)	AD (Å)	AA (°)
α-Glu-Aca			
(P309)O…HO-3C(Ring-A)	95.44	2.81	145.70
(D349)OD2…HO-3C(Ring-D)	66.43	2.81	152.15
(D349)OD2…HO-2C (Ring-D)	56.56	2.69	165.00
(Ring-D)3C-OH…HH12(R439)	42.48	3.00	151.22
(D349)OD1… HO-3C(Ring-D)	38.39	2.93	150.80
(Ring-C)6C-OH…HE(R312)	15.79	3.15	134.07
α-Glu-Car			
(D304)OD1…HO-7C	64.35	2.70	159.97
(E274)OE2…HO-2C	10.60	2.65	163.64

The analysis is continued by looking at the direct interaction between inhibitor and receptor through contact atoms and hydrogen bonds at the atomistic level. Based on interactions at the atomistic level, Aca experiences more intense interactions than Car. It is shown by the number of contact atoms and H-bonds in each system. In detail, Aca-α-Glu (atom contact: ~30 contacts and H-bond: ~6 bonds) and Car-α-Glu (atom contact: ~11 contacts and H-bond: ~2 bonds). Those results are the interactions presented and taken based on the percentage of occupancy (PO) ≥ 10%. Moreover, the H-bond in each complex is described in detail in Table 3. It can be seen that the major contribution to the H-bond interaction is in the –OH group (HBD) of each inhibitor. As we alluded to in the previous section. The presence of the –OH in the inhibitor can increase the chances of H-bond interactions.[64] In our focus on the Car, the presence of –OH groups in the carbazole region (7C-OH and 2C-OH) contributes to the H-bond to residues E274 and D304. Previously, in the molecular docking section, three bonds were measured, such as (i) 7C-OH…D304(OD1), (ii) 2C-OH…E274(OE2), and (iii) G157(HN)…2"C=O (Fig. S3 and Table S2). However, the MD simulation shows two bonds have PO ≥ 10%. In particular, the G157(HN)…2"C=O bond was also measured. However, it has a very small PO%, which is 0.81%. Thus, it is not feasible to be categorized as an H-bond because it is feeble. These results have answered our previous assumption that the Carbazol region provides a more dominant contribution to the H-bond interaction in the α-Glucosidase pocket area.

3.6 Inhibitory efficiency: Inhibitor against the α-Glucosidase

For inhibitory efficiency evaluation, we also calculate theoretical (ΔG_{bind}) and experimental (ΔG_{exp}) free energy binding. Mathematically, the value of each parameter is obtained from equations 9 and 10, as already mentioned in the previous section. Specifically, the ΔG_{bind} was calculated using the MM-PBSA approach at 100 frames of the last 20 ns

trajectories. This consideration was taken because the Aca-α-Glu and Car-α-Glu systems had achieved system stability in these regions (Fig. 6 and Table S2). In addition, the superposition of each inhibitor on the α-Glucosidase active site does not show a change in coordinates that is significant in the range of 180-200 ns last trajectories (Fig. 9). Finally, the energy components are listed in Table 4.

Table 4. Energy components (kcal/mol) of inhibitors-α-glucosidase complexes calculated with MM-PBSA approach. Data are shown as mean ± standard error of the mean (SEM).

Energy Components	α-Glu-Aca	α-Glu-Car
MM		
ΔE_{vdW}	-48.23 ± 0.64	-57.82 ± 0.37
ΔE_{ele}	-226.62 ± 2.11	-47.15 ± 0.90
ΔG_{gas}	-274.86 ± 1.85	-104.97 ± 0.85
Solvation (PBSA)		
ΔG_{solv}^{ele}	247.25 ± 1.73	79.35 ± 0.68
$\Delta G_{solv}^{nonpolar}$	-8.98 ± 0.01	-10.18 ± 0.01
$\Delta G_{sol\ (PBSA)}$	238.26 ± 1.73	69.16 ± 0.67
Enthalpy		
$\Delta H_{(MM-PBSA)}$	-36.59 ± 1.08	-35.81± 0.56
Entropy (NMODE)		
$-T\Delta S$	32.11 ± 1.82	9.71 ± 1.80
Binding Free Energy		
$\Delta G_{bind\ (MM-PBSA)}$	-4.48	-6.10
ΔG_{exp}	-3.17	-5.02

The energy component suggests that the energy contribution in the gas phase (ΔG_{gas}) is more variable than in the solvation phase (ΔG_{solv}). Consequently, the enthalpy value (ΔH) of each system changes significantly. It can be understood that there are quite favorable contributions in the energy of the van der Waals (ΔE_{vdW}) and electrostatic (ΔE_{ele}) components. These two energy components are the main stabilizing force for Aca and Car bindings toward the α-Glucosidase active site. Besides, the Poisson Boltzmann model (ΔG_{solv}^{ele}) shows a less beneficial interaction from the solvation phase. This contribution makes a significant difference to the ΔH value of each system. Moreover, the calculation of entropy change ($-T\Delta S$) owned by Car-α-Glu (9.71 ± 1.80 kcal/mol) is smaller than Aca-α-Glu (32.11 ± 1.82 kcal/mol). It is the contribution of ΔH and $-T\Delta S$ that causes the difference in ΔG_{bind} on the inhibitory efficiency of each inhibitor.[65,66]

Our findings show a good correlation between ΔG_{bind} and ΔG_{exp} values. It can be seen that the Car has a better inhibitory efficiency against α-Glucosidase than the Aca as a positive control. It is shown by the values of ΔG_{bind} and ΔG_{exp}, Car (ΔG_{bind}: -6.10 kcal/mol and ΔG_{exp}: -5.02 kcal/mol), which are smaller than Aca (ΔG_{bind}: -4.48 kcal/mol and ΔG_{exp}: -3.17 kcal/mol). Thermodynamically, a smaller free energy value indicates a stronger binding. This statement is acceptable because the stronger binding of the inhibitor is expected to inhibit the regulation of monosaccharide release through hydrolysis reactions at the α-Glucosidase active site.[39,62,66] Orientation inhibitors with strong free energy binding in the pocket area of α-Glucosidase are expected to be able to occupy their active sites so that they are not occupied by carbohydrate molecules (disaccharide and oligosaccharide). The goal is for the hydrolysis of carbohydrates by this enzyme can be stopped. In harmony, the *in vitro* tests that we have done previously suggested that new carbazomarin-C is a potential agent as an inhibitor of the α-Glucosidase enzyme compared to acarbose.[22]

Moreover, energy decomposition ($\Delta G_{bind}^{residue}$) was calculated to identify the key binding residues responsible for bond stabilization to inhibitors.[43,66] The selection of key

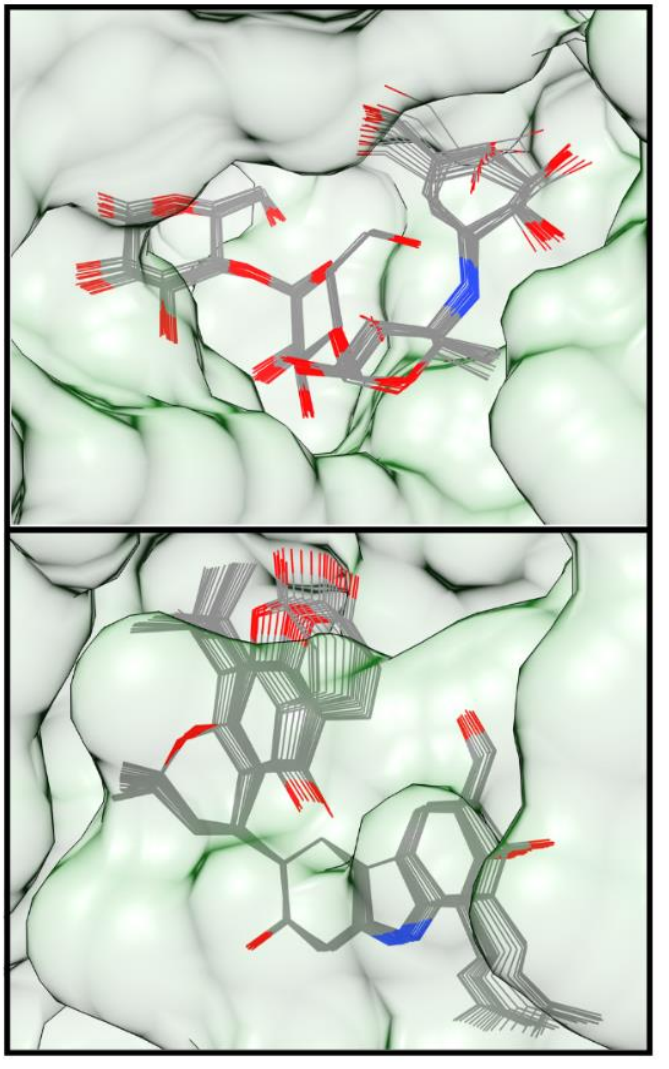

Fig. 9 The inhibitor superposition on the α-glucosidase pocket area was extracted in 20 snapshots from the last 20 ns trajectories: Aca-α-Glu (top) and Car-α-Glu (bottom).

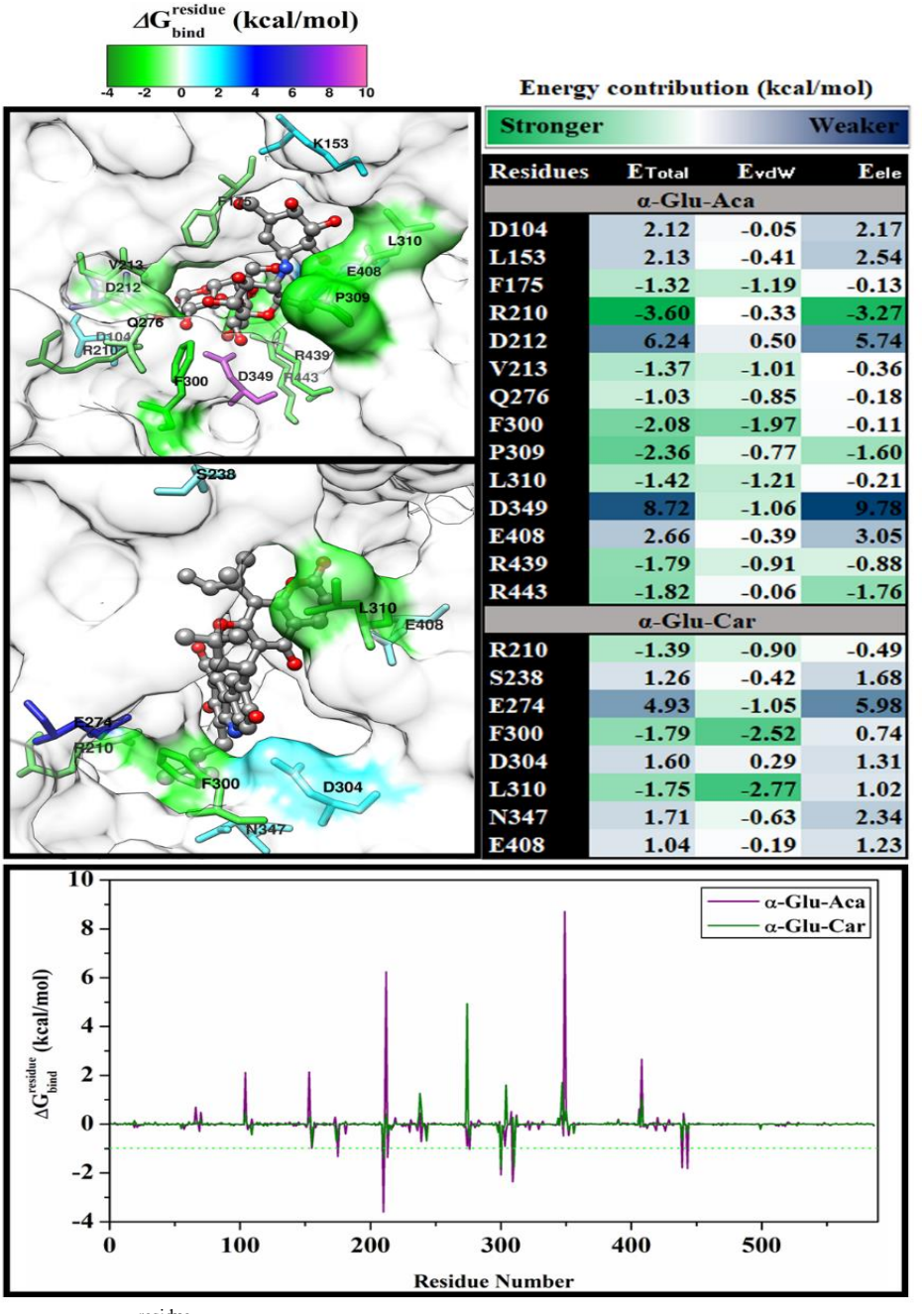

Residues	ETotal	EvdW	Eele
α-Glu-Aca			
D104	2.12	-0.05	2.17
L153	2.13	-0.41	2.54
F175	-1.32	-1.19	-0.13
R210	-3.60	-0.33	-3.27
D212	6.24	0.50	5.74
V213	-1.37	-1.01	-0.36
Q276	-1.03	-0.85	-0.18
F300	-2.08	-1.97	-0.11
P309	-2.36	-0.77	-1.60
L310	-1.42	-1.21	-0.21
D349	8.72	-1.06	9.78
E408	2.66	-0.39	3.05
R439	-1.79	-0.91	-0.88
R443	-1.82	-0.06	-1.76
α-Glu-Car			
R210	-1.39	-0.90	-0.49
S238	1.26	-0.42	1.68
E274	4.93	-1.05	5.98
F300	-1.79	-2.52	0.74
D304	1.60	0.29	1.31
L310	-1.75	-2.77	1.02
N347	1.71	-0.63	2.34
E408	1.04	-0.19	1.23

Fig. 10 Energy decomposition ($\Delta G_{bind}^{residue}$) and energy contribution (E_{vdW} and E_{ele}) were analyzed by the last 20 ns trajectories using the MM-PBSA approach.

binding residues is focused on amino acid residues with $\Delta G_{bind}^{residue} < -1.00$ kcal/mol.[39] These criteria indicate that the amino acid residues act as key binding residues. In detail, each system shows that several amino acid residues meet these criteria, followed by Aca-α-Glu (nine residues: F175, R210, V213, Q276, F300, P309, L310, R439, and R443) and Car- α-Glu (three residues: R210, F300, and L310) (Fig. 10). We suspect that three residues play a crucial role in the stabilization of the Aca and Car inhibitors, such as R210, F300, and L310. Our focus is on the orientation of the Car molecule, which gives the binding pattern to the α-Glucosidase pocket area. Once again, we mentioned that the combination of carbazol and coumarin made a good contribution in reaching several amino acid residues in the α-Glucosidase pocket. The similarity of the binding pattern is shown by Car and Aca. Both inhibitors are well occupied in the α-Glucosidase pocket area (Fig. 9). It is hoped that the key binding residue information presented will provide a clear picture of the stabilization of Car to α-Glucosidase at the molecular level.

All findings in this work show that the Carbazomarin-C molecule has a stronger binding to the active site of α-Glucosidase compared to acarbose as a control. These findings have the same correlation as the *in vitro* test of Carbazomarin-C (IC_{50}: 0.22 mM).[22] It should be noted that the α-Glucosidase

inhibitory activity of Carbazomarin-C has better potential than several known inhibitors, such as acarbose (4.89 mM)[22] and deoxynojirimycin (0.44 mM).[67] Furthermore, several inhibitors from the coumarin and alkaloid classes had inhibitory activity *in vitro* (IC_{50}), namely nordentatin: 36.70 mM,[25] xanthoxyletin: 4.81 mM,[22] oriciacridone C: 56.00 mM,[68] and oriciacridone F: 34.05 mM.[68] This finding proves that alkaloid and coumarin as the main structure of Carbazomarin-C can increase α-Glucosidase inhibitory activity. Another benefit of carbazomarin-C is well absorbed in the small intestine and non-toxic. It is known that acarbose cannot be absorbed in the small intestine and causes side effects, such as diarrhea and small intestine irritation.[69] Therefore, it can be considered for Carbazomarin-C as a promising α-Glucosidase inhibitor.

4. Conclusions

In this work, several computational studies were applied to elucidate the structural and molecular inhibitory properties of Carbazomarin-C (Car) to α-Glucosidase at the molecular level. The pharmacokinetic shows the criteria as a promising drug candidate by fulfilling the criteria of drug-likeness and non-toxic category. Meanwhile, proton chemical shift (^{1}H-NMR) modeling uses density functional theory (DFT). The results show that the ^{1}H-NMR correlation experimentally and theoretically has good forecasting of accuracy through statistical analysis. Furthermore, we studied the interaction between Carbazomarin-C and α-Glucosidase through a based-structure. From 200 ns during MD simulation, we studied dynamics behavior, interaction on the pocket area, and inhibitory efficiency. Dynamics behavior showed that each system achieved good stability and equilibrium for 200 ns simulation time. The carbazole region on the Car molecule contributes to the hydrogen bond interaction (PO ≥ 10%) in residues E274 and D304 in the form of HBD. Meanwhile, inhibitory efficiency shows consistent results between theoretical (ΔG_{bind}) and experimental (ΔG_{exp}) free energy binding. The results suggest that Car molecules have better inhibitory than the positive control Acarbose (Aca). We also identified that several key binding residues ($\Delta G^{residue}_{bind}$), such as R210, F300, and L310, are responsible for the stabilization of Car binding in the α-Glucosidase pocket area. Altogether, the obtained results from this work could be useful to understand the potential of Carbazomarin-C as an α-Glucosidase inhibitor and the development of some type of inhibitor from this structure in the future.

Acknowledgements

This study was supported by the Research Program of "Internasional Research Network (IRN)" from Universitas Airlangga. Contract Number: 1670/UN3.LPPM/PT.01.03/2023. Additionally, we are grateful for the computational resources for this work supported by UCoE Research Center for Bio-Molecule Engineering, Universitas Airlangga (BIOME-UNAIR) and Computational Drug Design Laboratorium (P-133), PCMD, ICCBS, University of Karachi.

Conflict of Interest

There is no conflict of interest.

Supporting Information

Applicable.

References

[1] R. Adela, S. K. Nethi, P. K. Bagul, A. K. Barui, S. Mattapally, M. Kuncha, C. R. Patra, P. N. C. Reddy, S. K. Banerjee, Hyperglycaemia enhances nitric oxide production in diabetes: a study from South Indian patients, *PLoS One*, 2015, **10**, e0125270, doi: 10.1371/journal.pone.0125270.

[2] K. Sharif, S. Ghadir, D. Jakubowicz, H. Amital, N. L. Bragazzi, A. Watad, J. Wainstein, Y. Bar-Dayan, Improved outcome of patients with diabetes mellitus with good glycemic control in the cardiac intensive care unit: a retrospective study, *Cardiovascular Diabetology*, 2019, **18**, 4, doi: 10.1186/s12933-019-0810-8.

[3] B. Giri, S. Dey, T. Das, M. Sarkar, J. Banerjee, S. K. Dash, Chronic hyperglycemia mediated physiological alteration and metabolic distortion leads to organ dysfunction, infection, cancer progression and other pathophysiological consequences: an update on glucose toxicity, *Biomedicine & Pharmacotherapy*, 2018, **107**, 306-328, doi: 10.1016/j.biopha.2018.07.157.

[4] G. Dimitriadis, P. Mitrou, V. Lambadiari, E. Maratou, S. A. Raptis, Insulin effects in muscle and adipose tissue, *Diabetes Research and Clinical Practice*, 2011, **93**, S52-S59, doi: 10.1016/s0168-8227(11)70014-6.

[5] T. R. Einarson, A. Acs, C. Ludwig, U. H. Panton, Prevalence of cardiovascular disease in type 2 diabetes: a systematic literature review of scientific evidence from across the world in 2007–2017, *Cardiovascular Diabetology*, 2018, **17**, 83, doi: 10.1186/s12933-018-0728-6.

[6] C. C. Low Wang, C. N. Hess, W. R. Hiatt, A. B. Goldfine, Clinical update: cardiovascular disease in diabetes mellitus: atherosclerotic cardiovascular disease and heart failure in type 2 diabetes mellitus - mechanisms, management, and clinical considerations, *Circulation*, 2016, **133**, 2459-2502, doi: 10.1161/CIRCULATIONAHA.116.022194.

[7] T. Penlioglou, A. P. Stoian, N. Papanas, Diabetes, vascular aging and stroke: old dogs, new tricks? *Journal of Clinical Medicine*, 2021, **10**, 4620, doi: 10.3390/jcm10194620.

[8] C. I. Chukwuma, M. G. Matsabisa, M. A. Ibrahim, O. L. Erukainure, M. H. Chabalala, M. S. Islam, Medicinal plants with concomitant anti-diabetic and anti-hypertensive effects as potential sources of dual acting therapies against diabetes and hypertension: a review, *Journal of Ethnopharmacology*, 2019, **235**, 329-360, doi: 10.1016/j.jep.2019.02.024.

[9] F. Rivero-Pino, F. J. Espejo-Carpio, E. M. Guadix, Production

and identification of dipeptidyl peptidase IV (DPP-IV) inhibitory peptides from discarded Sardine pilchardus protein, *Food Chemistry*, 2020, **328**, 127096, doi: 10.1016/j.foodchem.2020.127096.
[10] H. Kashtoh, K.-H. Baek, Recent updates on phytoconstituent alpha-glucosidase inhibitors: an approach towards the treatment of type two diabetes, *Plants*, 2022, **11**, 2722, doi: 10.3390/plants11202722.
[11] N. Kaur, V. Kumar, S. K. Nayak, P. Wadhwa, P. Kaur, S. K. Sahu, Alpha-amylase as molecular target for treatment of diabetes mellitus: a comprehensive review, *Chemical Biology & Drug Design*, 2021, **98**, 539-560, doi: 10.1111/cbdd.13909.
[12] F. Pan, N. Zhou, J. Li, X. Du, L. Zhao, C. Wang, M. Zhang, X. Ai, Identification of C-phycocyanin-derived peptides as angiotensin converting enzyme and dipeptidyl peptidase IV inhibitors via molecular docking and molecular dynamic simulation, *ES Food & Agroforestry*, 2020, **2**, 58-67, doi: 10.30919/esfaf1116.
[13] A. Kicel, A. Magiera, M. Skrzywanek, M. Malczuk, M. A. Olszewska, The inhibition of α-glucosidase, α-amylase and protein glycation by phenolic extracts of cotoneaster bullatus, cotoneaster zabelii, and cotoneaster integerrimus leaves and fruits: focus on anti-hyperglycemic activity and kinetic parameters, *Molecules*, 2022, **27**, 7081, doi: 10.3390/molecules27207081.
[14] T. Tian, G. Y. Chen, H. Zhang, F. Q. Yang, Personal glucose meter for α-glucosidase inhibitor screening based on the hydrolysis of maltose, *Molecules* 2021, **26**, 1-11, doi: 10.3390/molecules26154638.
[15] S. Padhi, A. K. Nayak, A. Behera, Type II diabetes mellitus: a review on recent drug based therapeutics, *Biomedicine & Pharmacotherapy*, 2020, **131**, 110708, doi: 10.1016/j.biopha.2020.110708.
[16] C. Zhao, X. Wan, S. Zhou, H. Cao, Natural polyphenols: a potential therapeutic approach to hypoglycemia, *eFood*, 2020, **1**, 107-118, doi: 10.2991/efood.k.200302.001.
[17] Z. Liu, J. Gong, W. Huang, F. Lu, H. Dong, The effect of momordica charantia in the treatment of diabetes mellitus: a review, *Evidence-Based Complementary and Alternative Medicine*, 2021, **2021**, 3796265, doi: 10.1155/2021/3796265.
[18] U. Hossain, A. K. Das, S. Ghosh, P. C. Sil, An overview on the role of bioactive α-glucosidase inhibitors in ameliorating diabetic complications, *Food and Chemical Toxicology*, 2020, **145**, 111738, doi: 10.1016/j.fct.2020.111738.
[19] S. T. Assefa, E.-Y. Yang, S.-Y. Chae, M. Song, J. Lee, M.-C. Cho, S. Jang, Alpha glucosidase inhibitory activities of plants with focus on common vegetables, *Plants*, 2019, **9**, 2, doi: 10.3390/plants9010002.
[20] J. J. DiNicolantonio, J. Bhutani, J. H. O'Keefe, Acarbose: safe and effective for lowering postprandial hyperglycaemia and improving cardiovascular outcomes, *Open Heart*, 2015, **2**, e000327, doi: 10.1136/openhrt-2015-000327.
[21] L. Gong, D. Feng, T. Wang, Y. Ren, Y. Liu, J. Wang, Inhibitors of α-amylase and α-glucosidase: potential linkage for whole cereal foods on prevention of hyperglycemia, *Food Science & Nutrition*, 2020, **8**, 6320-6337, doi: 10.1002/fsn3.1987.
[22] N. S. Aminah, T. M. Thant, A. N. Kristanti, R. Ramadhan, H. T. Aung, Y. Takaya, Carbazomarin: A new potential of α-glucosidase inhibitor from *Clausena excavata* roots, *Natural Product Communications*, 2019, **14**, 1-6, doi: 10.1177/1934578x19894076.
[23] P. Ertl, E. Altmann, J. M. Mckenna, The most common functional groups in bioactive molecules and how their popularity has evolved over time, *Journal of Medicinal Chemistry*, 2020, **63**, 8408-8418, doi: 10.1021/acs.jmedchem.0c00754.
[24] T. M. Thant, N. S. Aminah, A. N. Kristanti, R. Ramadhan, P. Phuwapraisirisan, Y. Takaya, A new pyrano coumarin from *Clausena excavata*roots displaying dual inhibition against α-glucosidase and free radical, *Natural Product Research*, 2021, **35**, 556-561, doi: 10.1080/14786419.2019.1586696.
[25] T. M. Thant, N. S. Aminah, A. N. Kristanti, R. Ramadhan, H. T. Aung, Y. Takaya, New derivatives of a natural nordentatin, *Open Chemistry*, 2020, 18, 890-897, doi: 10.1515/chem-2020-0149.
[26] S. N. T. I. Sampath, S. Jayasinghe, A. P. Attanayake, V. Karunaratne, M. L. Yaddehige, D. L. Watkins, A new dimeric carbazole alkaloid from Murraya koenigii (L.) leaves with α-amylase and α-glucosidase inhibitory activities, *Phytochemistry Letters*, 2022, **52**, 87-91, doi: 10.1016/j.phytol.2022.09.013.
[27] C. Proença, M. Freitas, D. Ribeiro, E. F. T. Oliveira, J. L. C. Sousa, S. M. Tomé, M. J. Ramos, A. M. S. Silva, P. A. Fernandes, E. Fernandes, α-Glucosidase inhibition by flavonoids: an*in vitro*and*in silico*structure–activity relationship study, *Journal of Enzyme Inhibition and Medicinal Chemistry*, 2017, **32**, 1216-1228, doi: 10.1080/14756366.2017.1368503.
[28] H. Chenafa, F. Mesli, I. Daoud, R. Achiri, S. Ghalem, A. Neghra, In silico design of enzyme α-amylase and α-glucosidase inhibitors using molecular docking, molecular dynamic, conceptual DFT investigation and pharmacophore modelling, *Journal of Biomolecular Structure and Dynamics*, 2022, **40**, 6308-6329, doi: 10.1080/07391102.2021.1882340.
[29] M. Bitew, T. Desalegn, T. B. Demissie, A. Belayneh, M. Endale, R. Eswaramoorthy, Pharmacokinetics and drug-likeness of antidiabetic flavonoids: molecular docking and DFT study, *PLoS One*, 2021, **16**, e0260853, doi: 10.1371/journal.pone.0260853.
[30] M. A. B. Macalalad, A. A. Gonzales III, In-silico screening and identification of phytochemicals from*Centella asiatica*as potential inhibitors of sodium-glucose co-transporter 2 for treating diabetes, *Journal of Biomolecular Structure and Dynamics*, 2022, **40**, 12221-12238, doi: 10.1080/07391102.2021.1969282.
[31] D. E. V. Pires, T. L. Blundell, D. B. Ascher, pkCSM: predicting small-molecule pharmacokinetic and toxicity properties using graph-based signatures, *Journal of Medicinal Chemistry*, 2015, **58**, 4066-4072, doi: 10.1021/acs.jmedchem.5b00104.
[32] A. Daina, O. Michielin, V. Zoete, SwissADME: a free web tool to evaluate pharmacokinetics, drug-likeness and medicinal chemistry friendliness of small molecules, *Scientific Reports*, 2017, **7**, 42717, doi: 10.1038/srep42717.

[33] P. Geerlings, F. De Proft, Chemical reactivity as described by quantum chemical methods, *International Journal of Molecular Sciences*, 2002, **3**, 276-309, doi: 10.3390/i3040276.
[34] A. D. Becke, Density-functional thermochemistry. III. The role of exact exchange, *The Journal of Chemical Physics*, 1993, **98**, 5648-5652, doi: 10.1063/1.464913.
[35] K. Wolinski, J. F. Hinton, P. Pulay, Efficient implementation of the gauge-independent atomic orbital method for NMR chemical shift calculations, *Journal of the American Chemical Society*, 1990, **112**, 8251-8260, doi: 10.1021/ja00179a005.
[36], M. I. Abdjan, N. S. Aminah, A. N. Kristanti, I. Siswanto, M. A. Saputra, Y. Takaya, Pharmacokinetic, DFT modeling, molecular docking, and molecular dynamics simulation approaches: diptoindonesin A as a potential inhibitor of sirtuin-1, *Engineered Science*, 2023, **21**, 794, doi: 10.30919/es8d794.
[37] L. A. De Souza, H. C. Da Silva, W. B. De Almeida, Structural determination of antioxidant and anticancer flavonoid rutin in solution through DFT calculations of 1H NMR chemical shifts, *ChemistryOpen*, 2018, **7**, 902-913, doi: 10.1002/open.201800209.
[38] K. Yamamoto, H. Miyake, M. Kusunoki, S. Osaki, Crystal structures of isomaltase from Saccharomyces cerevisiae and in complex with its competitive inhibitor maltose, *The FEBS Journal*, 2010, **277**, 4205-4214, doi: 10.1111/j.1742-4658.2010.07810.x.
[39] M. I. Abdjan, N. S. Aminah, A. N. Kristanti, I. Siswanto, B. Ilham, A. P. Wardana, Y. Takaya, Structure-based approach: molecular insight of pyranocumarins against α-glucosidase through computational studies, *RSC Advances*, 2023, **13**, 3438-3447, doi: 10.1039/d2ra07537g.
[40] S. R. Brozell, S. Mukherjee, T. E. Balius, D. R. Rze, D. A. Case, R. C. Rizzo, Evaluation of DOCK 6 as a pose generation and database enrichment tool, *Journal of Computer-Aided Molecular Design*, 2012, **26**, 749-773, doi: 10.1007/s10822-012-9565-y.
[41] W. J. Allen, T. E. Balius, S. Mukherjee, S. R. Brozell, D. T. Moustakas, P. T. Lang, D. A. Case, I. D. Kuntz, R. C. Rizzo, DOCK 6: impact of new features and current docking performance, *Journal of Computational Chemistry*, 2015, **36**, 1132-1156, doi: 10.1002/jcc.23905.
[42] Z.-W. Zhang, W.-C. Lu, AmberMDrun: A scripting tool for running amber MD in an easy way, *Biomolecules*, 2023, **13**, 635, doi: 10.3390/biom13040635.
[43] B. Nutho, S. Pengthaisong, A. Tankrathok, V. S. Lee, J. R. Ketudat Cairns, T. Rungrotmongkol, S. Hannongbua, Structural basis of specific glucoimidazole and mannoimidazole binding by Os3BGlu7, *Biomolecules*, 2020, **10**, 907, doi: 10.3390/biom10060907.
[44] D. A. Case, T. E. Cheatham III, T. Darden, H. Gohlke, R. Luo, K. M. Merz Jr., A. Onufriev, C. Simmerling, B. Wang, R. J. Woods, The Amber biomolecular simulation programs, *Journal of Computational Chemistry*, 2005, **26**, 1668-1688, doi: 10.1002/jcc.20290.
[45] T.-S. Lee, D. S. Cerutti, D. Mermelstein, C. Lin, S. LeGrand, T. J. Giese, A. Roitberg, D. A. Case, R. C. Walker, D. M. York, GPU-accelerated molecular dynamics and free energy methods in Amber18: performance enhancements and new features, *Journal of Chemical Information and Modeling*, 2018, **58**, 2043-2050, doi: 10.1021/acs.jcim.8b00462.
[46] M. Chrabąszczewska, A. K. Sieradzan, S. Rodziewicz-Motowidło, A. Grubb, C. M. Dobson, J. R. Kumita, M. Kozak, Structural characterization of covalently stabilized human cystatin C oligomers, *International Journal of Molecular Sciences*, 2020, **21**, 5860, doi: 10.3390/ijms21165860.
[47] D. R. Roe, T. E. Cheatham III, PTRAJ and CPPTRAJ: software for processing and analysis of molecular dynamics trajectory data, *Journal of Chemical Theory and Computation*, 2013, **9**, 3084-3095, doi: 10.1021/ct400341p.
[48] B. R. Miller III, T. D. McGee Jr, J. M. Swails, N. Homeyer, H. Gohlke, A. E. Roitberg, *MMPBSA.py*: an efficient program for end-state free energy calculations, *Journal of Chemical Theory and Computation*, 2012, **8**, 3314-3321, doi: 10.1021/ct300418h.
[49] X. Hu, A. Contini, Rescoring virtual screening results with the MM-PBSA methods: beware of internal dielectric constants, *Journal of Chemical Information and Modeling*, 2019, **59**, 2714-2728, doi: 10.1021/acs.jcim.9b00095.
[50] W. M. Menzer, C. Li, W. Sun, B. Xie, D. D. L. Minh, Simple entropy terms for end-point binding free energy calculations, *Journal of Chemical Theory and Computation*, 2018, **14**, 6035-6049, doi: 10.1021/acs.jctc.8b00418.
[51] H. C. Cheng, The power issue: determination of K_B or K_i from IC_{50}: A closer look at the Cheng–Prusoff equation, the Schild plot and related power equations, *Journal of Pharmacological and Toxicological Methods*, 2001, **46**, 61-71, doi: 10.1016/S1056-8719(02)00166-1.
[52] C. A. Lipinski, F. Lombardo, B. W. Dominy, P. J. Feeney, Experimental and computational approaches to estimate solubility and permeability in drug discovery and development settings, *Advanced Drug Delivery Reviews*, 2012, **64**, 4-17, doi: 10.1016/j.addr.2012.09.019.
[53] D. F. Veber, S. R. Johnson, H.-Y. Cheng, B. R. Smith, K. W. Ward, K. D. Kopple, Molecular properties that influence the oral bioavailability of drug candidates, *Journal of Medicinal Chemistry*, 2002, **45**, 2615-2623, doi: 10.1021/jm020017n.
[54] J. Ziemska, J. Solecka, M. Jarończyk, In Silico Screening for Novel Leucine Aminopeptidase Inhibitors with 3,4-Dihydroisoquinoline Scaffold, *Molecules*, 2020, **25**, 1-16 doi: 10.3390/molecules25071753.
[55] R. N. Guzzo, M. J. C. Rezende, V. Kartnaller, J. W. de M. Carneiro, S. R. Stoyanov, L. M. da Costa, Experimental and DFT evaluation of the 1H and ^{13}C NMR chemical shifts for calix[4]arenes, *Journal of Molecular Structure*, 2018, **1157**, 97-105, doi: 10.1016/j.molstruc.2017.12.038.
[56] X.-Y. Meng, H.-X. Zhang, M. Mezei, M. Cui, Molecular docking: a powerful approach for structure-based drug discovery, *Current Computer Aided-Drug Design*, 2011, **7**, 146-157, doi: 10.2174/157340911795677602.
[57] A. Vidal-Limon, J. E. Aguilar-Toalá, A. M. Liceaga, Integration of molecular docking analysis and molecular dynamics simulations for studying food proteins and bioactive

peptides, *Journal of Agricultural and Food Chemistry*, 2022, **70**, 934-943, doi: 10.1021/acs.jafc.1c06110.
[58] J. Wang, R. M. Wolf, J. W. Caldwell, P. A. Kollman, D. A. Case, Development and testing of a general amber force field, *Journal of Computational Chemistry*, 2004, **25**, 1157-1174, doi: 10.1002/jcc.20035.
[59] S. Kongkaew, P. Yotmanee, T. Rungrotmongkol, N. Kaiyawet, A. Meeprasert, T. Kaburaki, H. Noguchi, F. Takeuchi, N. Kungwan, S. Hannongbua, Molecular dynamics simulation reveals the selective binding of human leukocyte antigen alleles associated with behçet's disease, *PLoS One*, 2015, **10**, e0135575, doi: 10.1371/journal.pone.0135575.
[60] A. Bornot, C. Etchebest, A. G. de Brevern, Predicting protein flexibility through the prediction of local structures, *Proteins: Structure, Function, and Bioinformatics*, 2011, **79**, 839-852, doi: 10.1002/prot.22922.
[61] M. Y. Lobanov, N. S. Bogatyreva, O. V. Galzitskaya, Radius of gyration as an indicator of protein structure compactness, *Molecular Biology*, 2008, **42**, 623-628, doi: 10.1134/s0026893308040195.
[62] X. Zheng, H. Chi, S. Ma, L. Zhao, S. Cai, Identification of novel α-glucosidase inhibitory peptides in rice wine and their antioxidant activities using in silico and *in vitro* analyses, *LWT*, 2023, **178**, 114629, doi: 10.1016/j.lwt.2023.114629.
[63] T. Vajda, A. Perczel, Role of water in protein folding, oligomerization, amyloidosis and miniprotein, *Journal of Peptide Science*, 2014, **20**, 747-759, doi: 10.1002/psc.2671.
[64] S. Y. Mohamed, M. Monge-Palacios, B. R. Giri, F. Khaled, D. Liu, A. Farooq, S. M. Sarathy, The effect of hydrogen bonding on the reactivity of OH radicals with prenol and isoprenol: a shock tube and multi-structural torsional variational transition state theory study, *Physical Chemistry Chemical Physics*, 2022, **24**, 12601-12620, doi: 10.1039/d2cp00737a.
[65] K. V. Presnell, H. S. Alper, Thermodynamic and first-principles biomolecular simulations applied to synthetic biology: promoter and aptamer designs, *Molecular Systems Design & Engineering*, 2018, **3**, 19-37, doi: 10.1039/c7me00083a.
[66] E. Wang, H. Sun, J. Wang, Z. Wang, H. Liu, J. Z. H. Zhang, T. Hou, End-point binding free energy calculation with MM/PBSA and MM/GBSA: strategies and applications in drug design, *Chemical Reviews*, 2019, **119**, 9478-9508, doi: 10.1021/acs.chemrev.9b00055.
[67] S. Maher, M. I. Choudhary, F. Saleem, S. Rasheed, I. Waheed, S. A. Halim, M. Azeem, I. Bin Abdullah, M. Froeyen, M. U. Mirza, S. Ahmad, Isolation of antidiabetic withanolides from withania coagulans dunal and their *in vitro* and in silico validation, *Biology*, 2020, **9**, 197, doi: 10.3390/biology9080197.
[68] J. D. Wansi, J. Wandji, L. Mbaze Meva'a, A. F. Kamdem Waffo, R. Ranjit, S. N. Khan, A. Asma, C. M. Iqbal, M.-C. Lallemand, F. Tillequin, Z. Fomum Tanee, .ALPHA.-glucosidase inhibitory and antioxidant acridone alkaloids from the stem bark of oriciopsis glaberrima ENGL. (rutaceae), *Chemical and Pharmaceutical Bulletin*, 2006, **54**, 292-296, doi: 10.1248/cpb.54.292.
[69] R. E. Kast, Acarbose related diarrhea: increased butyrate upregulates prostaglandin E, *Inflammation Research*, 2002, **51**, 117-118, doi: 10.1007/PL00012389.